

Self-referenced Readout of Nanopore Translocation Signals Using Localized Electrometry

Muhammad Sajeer P, Manoj Varma.*

Center for Nanoscience and Engineering, Indian Institute of Science, Bangalore

KEYWORDS: DNA and protein sequencing , Solid-state nanopores, nanopore electrometry, electric field sensing, ionic current blockade-based sensing,

Table of Contents

| | |
|--|----|
| Abstract | 2 |
| Introduction..... | 2 |
| Methods..... | 6 |
| Results and Discussion | 9 |
| Conclusion | 14 |
| Impact of research in the advancement of knowledge or benefit to mankind | 15 |
| Author information | 16 |
| Reference | 16 |

Abstract

For the past two decades, the ionic current blockade-based readout approach has been the basis of nanopore single-molecule sensing technology. Here, we introduce “nanopore electrometry,” a readout method based on measuring the modulation of the local electric field due to the translocation of the target molecule. Through comprehensive computational studies, we establish unique strengths of nanopore electrometry that can open up new frontiers in nanopore based molecular detection. For instance, electric field concentration inside the nanopore combined with the rapid decay of the field due to charge screening leads to asymmetric sensitivity of nanopore electrometry to the charge of the target, i.e. it can selectively detect cations or anions depending on the location of the electric field sensor or the direction of the external electric field. Further, simultaneous measurements from multiple local electric field sensors can be utilized for self-referenced error correction and to compensate for translocation velocity fluctuations. Nanopore electrometry can also be used to detect translocations without requiring liquid electrolytes. This study lays the foundation for the application of nanopore electrometry as a viable readout method.

Introduction

Solid-state nanopores are a promising alternative to biological nanopores due to their potential benefits, such as increased chemical, mechanical, and thermal stability. However, endeavors to accomplish DNA and protein sequencing using solid-state nanopores in the last two decades have encountered major challenges, such as, achieving precise translocation control, pore-to-pore variability, and spatio-temporal resolution^{1,2}. Nonetheless, solid-state nanopores have found utility in various applications, ranging from quality assurance³ and biomarker identification⁴ to DNA computing⁵. Solid-state nanopores consist of nanometer-scale pores of varying shapes, typically ranging from 1 to 100 nm in diameter, fabricated on ultra-thin solid membranes, usually with a

thickness ranging from 0.3 – 50 nm⁶. The membrane containing nanopores is sandwiched between two electrolyte-filled chambers, causing an ionic current to flow through the pore upon the application of a voltage bias across the chambers. Molecules translocating through the nanopore are identified based on characteristic alterations in ionic current—a technique referred to as ionic current blockade-based sensing. Currently, ionic current blockade-based measurement serves as the primary nanopore readout method and is even employed in commercial nanopore-based DNA sequencing devices⁷.

While ionic current blockade readout has been successfully demonstrated in various reports and commercial DNA sequencing, there are fundamental limitations of this technique that justify the exploration of alternate measurement methods. Firstly, there is a trade-off between measurement resolution and the measurement speed. This trade-off is fundamentally limited by the transport rate of charge carriers. When the measurement rate is increased, the number of carriers contributing to each measurement reduces, leading to large fluctuations in addition to other noises present in the system. Practically, this aspect limits the maximum rate at which information can be reliably extracted from nanopore data to about 1-10 kHz. For instance, a single biological pore used in DNA sequencing operates at about 0.5 kHz, achieved by using a motor protein to drive DNA translocation instead of the electric field near the nanopore⁸. For solid-state nanopores devoid of well-established techniques to slow down DNA translocation, the measurement rate limitation implies that most of the translocations are outside the detection range of the system. Another limitation of existing ionic current based readout is the limited complexity of the signal. The magnitude of the ionic blockade current is primarily determined by the pore volume excluded by the translocating molecule⁹. In addition, there may be effects from charged groups that may be present in the translocating molecule. Even in this case, the ionic current will be more strongly

correlated to the average charge density and average molecular volume rather than the actual heterogeneities in charge distribution or shape. This limited complexity may restrict the performance of ionic current based methods in emerging applications such as protein sequencing and glycomics due to the significantly enhanced complexities of target molecules in these applications relative to DNA or RNA¹⁰. Finally, ionic current methods require an electrolyte to provide the ions. This requirement directly precludes applications such as direct detection of viruses and other targets in ambient air¹¹. Electrolytes also limit potential applications in extreme environments. These are fundamental limitations of ionic current based nanopore readout aside from other practical considerations, such as the interaction of electrolyte with the sample or the pore^{12,13}. These limitations provide sufficient motivation to explore alternate nanopore readout strategies.

In this computational study, we explored “nanopore electrometry”, a readout method based on measuring the modulation of the local electric field due to the translocation of the target molecule **[Figure 1]**. The local electric field inherently exhibits sensitivity to the charge distribution of the target molecule, potentially encoding a wealth of information about the molecular characteristics. Thus, nanopore electrometry signals could possess significantly higher information capacity compared to conventional ionic current methods. Further, electric field-based readout does not require an electrolyte, rendering it amenable to extreme environments. This approach could also enable ambient-air monitoring for air-borne targets such as viruses using nanopores, solving the challenge highlighted by Kawai et al¹¹. Electric field sensing is currently well-established and widely employed as proximity and object identifier sensors at fairly large spatial scales^{14–17}. However, nanopore signal readout using electric-field modulations will require highly localized measurements. We expect that the recent development of nano¹⁸ and micro-scale¹⁹ electric field

sensors, nanoscale electric field imaging using nitrogen-vacancy (NV) center²⁰ and single spins²¹ present exciting prospects for their application in nanopore electrometry. Notably, a recent study has experimentally demonstrated the sensing of the electric field in a liquid electrolyte using NV centers in nanodiamonds²². These advancements indicate a potential pathway for the experimental realization of nanopore electrometric readout.

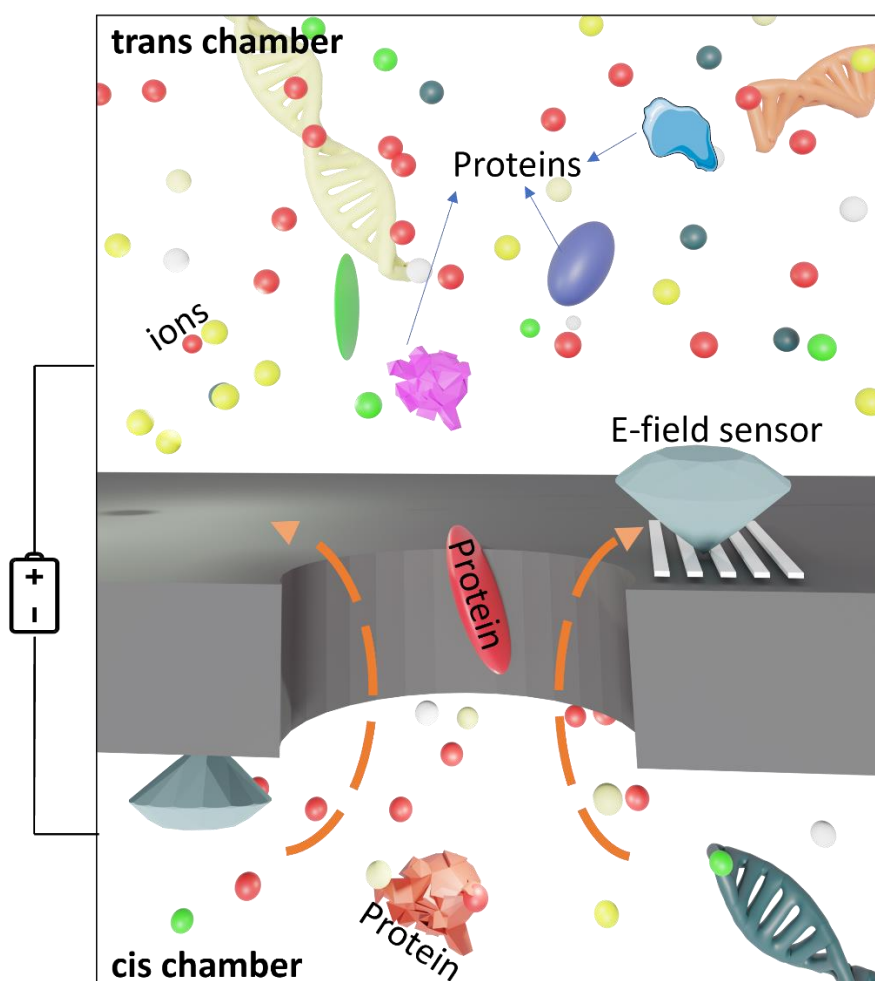


Figure 1. A schematic representation of nanopore electrometry based readout. Here, the nitrogen vacancy centres in nanodiamonds are used to sense the local electric field. The arrow indicate translocation from cis to trans chamber.

To explore the feasibility of nanopore electrometric readout, we used finite element simulations of particle translocating through a Silicon Nitride nanopore to estimate the local electric field magnitude at the entrance, exit and center of the nanopore (**Error! Reference source not found.A**). These simulations allowed us to compare the performance of nanopore electrometry relative to ionic current based readout. Nanopore electrometry has comparable sensitivity to ionic current readout for particle size and charge. Interestingly, electrometric signal can be made selective to cations or anions by controlling the position of the electric field sensor or the direction of external electric field. Most significantly, the localized measurement enables the nanopore electrometry signal to be used for self-referencing. This property allows for error correction and internal signal calibration. We discuss these aspects in greater detail in this paper.

Methods

We performed finite element simulations for nanopore by solving the Poisson-Nernst-Planck (PNP) equation in COMSOL (version 5.5). The COMSOL simulations are well known to reliably predict the experimental results and properties of nanopore systems^{23–26}. Our 2D axisymmetric model contains an hourglass-shaped silicon nitride nanopore with a length (L_p) of 10 nm, an entrance and exit with a diameter of 5 nm, and a central constriction of 3 nm (**Figure 2A**). We designated the center of the pore as the origin (0,0) and normalized the pore axial dimension (z-axis) by dividing it by the pore length (L_p), i.e. $z_{norm} = z/L_p$.

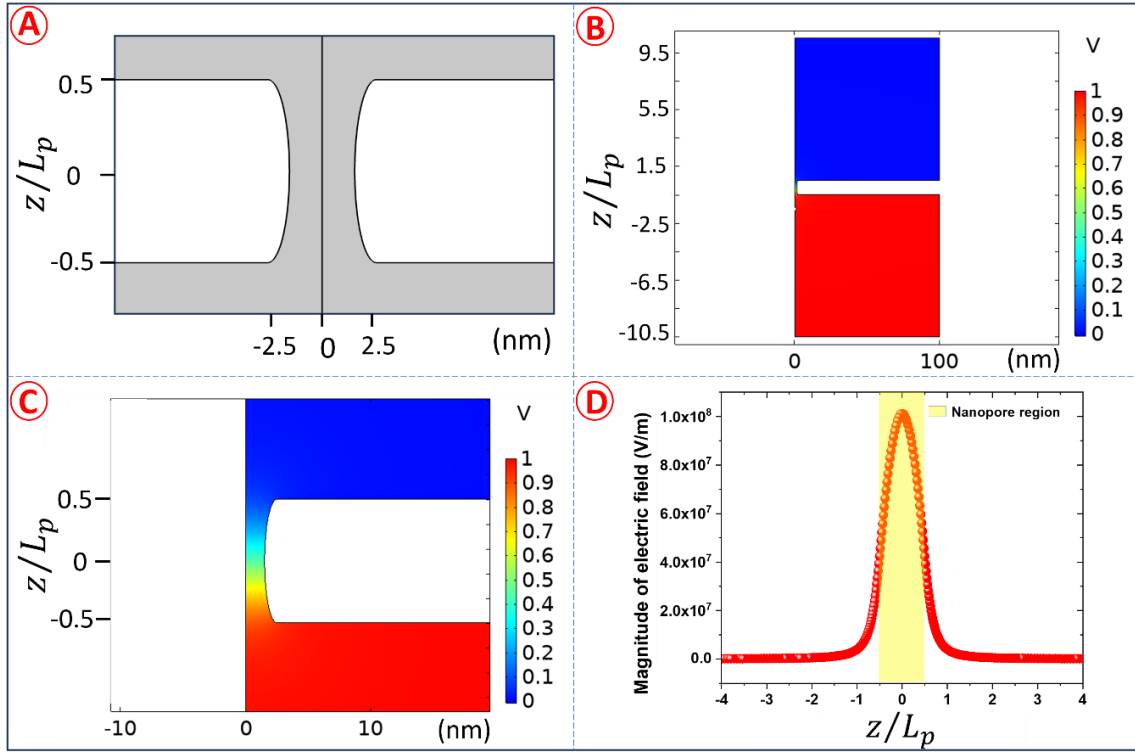


Figure 2. A) Hourglass-shaped solid state nanopore geometry created in COMSOL. B) Voltage distribution in the simulation volume, C) Magnified view of the voltage distribution near the nanopore D) Magnitude of the electric field along the central axis (z -axis) with highlighted region denoting nanopore boundaries. The maximum electric field is concentrated near the pore, rapidly diminishing away from it.

The nanopore is connected to two reservoirs containing 1M potassium chloride electrolyte. A nanoparticle, modeled as a sphere, is translocated along the Z -axis by incrementing the particle position in a step-wise manner. A voltage bias of 1V is applied between the reservoirs. **Figure 2(B-C)** shows the voltage distribution across the nanopore. **Figure 2D** indicates that the electric field is highly concentrated near the pore. Further details of the simulation model (parameters, boundary condition, meshing) are explained in detail in sections 1 and 2 of the supplementary information (SI).

To measure the local electric field (E-field), we calculated the magnitude of the electric field vector at the entry, exit, and center of the nanopore using the equation $\sqrt{E_r^2 + E_\phi^2 + E_z^2}$ where E_r, E_ϕ, E_z represents the r, ϕ , z components of E-field vector with unit V/m. From now on, the sensors located at the nanopore's entry, exit, and center will be referred to as the top edge sensor, bottom edge sensor, and center sensor, respectively. To understand the changes in the electric field sensor during the particle translocation, we define a ‘normalized signal contrast’, for the electric-field signal, denoted by $\gamma_E = \frac{\Delta E}{E_b}$. Here, ΔE is the change in the electric field signal with respect to the base line electric field (E_b) during the translocation of particles through the pore. The value of the base line electric field (E_b) is the background electric field during the absence of particle translocation through the pore. The base line electric field, E_b is analogous to the base line current in ionic current blockade sensing. From the normalized signal contrast, γ_E , one can obtain the maximum signal contrast, γ_E^{max} defined as the maximum of the absolute value of γ_E . Similarly, for comparison, we can define the normalized signal contrast value for the ionic current blockade sensing denoted by $\gamma_I = \frac{\Delta I}{I_b}$. Here, ΔI is the change in ionic current with respect to the base line current (I_b), which is commonly referred as the depth of ionic current blockade signal in the nanopore literature. The ionic current is calculated in COMSOL by defining a cross-sectional area (S) halfway through the pore and by doing a surface integration as per equation 1.

$$I = N_A e \iint (J_{K^+} - J_{Cl^-}) \cdot dS \quad (\text{Equation 1})$$

Here, N_A is the Avogadro number, e is the unit charge, and J represents the flux density of K^+ and Cl^- ions. The details are given in section 1 of the supplementary information. Corresponding to γ_E^{max} , one can define γ_I^{max} to represent the maximum signal contrast of the ionic current readout.

Results and Discussion

The size of the translocating molecule significantly influences the magnitude of the current blockade (ΔI) due to volume exclusion in the pore. **Figure 3A** illustrates the change in γ_I^{max} as particles having a homogeneous charge density ($\pm 50 \text{ mC/m}^2$) with diameters (D_p) ranging from 0.5 nm to 2.5 nm, translocate through the pore at a bias of 1 V. As anticipated, the current contrast increases proportionally with particle size. The slope of the log-log plot of ionic current against particle diameter for uncharged particles and uncharged pores (**Figure 3A**) yields a scaling factor close to 3 (3.12 ± 0.14), indicating a volume dominated effect on the ionic current blockade. This scale factor of 3 is further reduced to 2.27 ± 0.10 and 2.19 ± 0.06 when the particle ($\pm 50 \text{ mC/m}^2$) and pore (-23 mC/m^2) is charged indicating the role of electrostatic screening. The variation in scale factor for ionic current blockade for different scenarios is provided in **SI Figure 5**.

To explore the sensitivity of nanopore electrometry to particle size, we plotted the electric field signal contrast, γ_E^{max} , as a function of particle diameter. As shown in **Figure 3C, 3D** local electric field is indeed sensitive to the particle size. However, the sensitivity depends on the location of the sensor. The scaling factor of the signal contrast with diameter is close to 3 for the center sensor whereas it is around 1 for the top and bottom edge sensor, at a pore charge of -23 mC/m^2 [**Table 2 in SI**]. These differences between center and edge sensors arise from differences in the local field profiles at these locations.

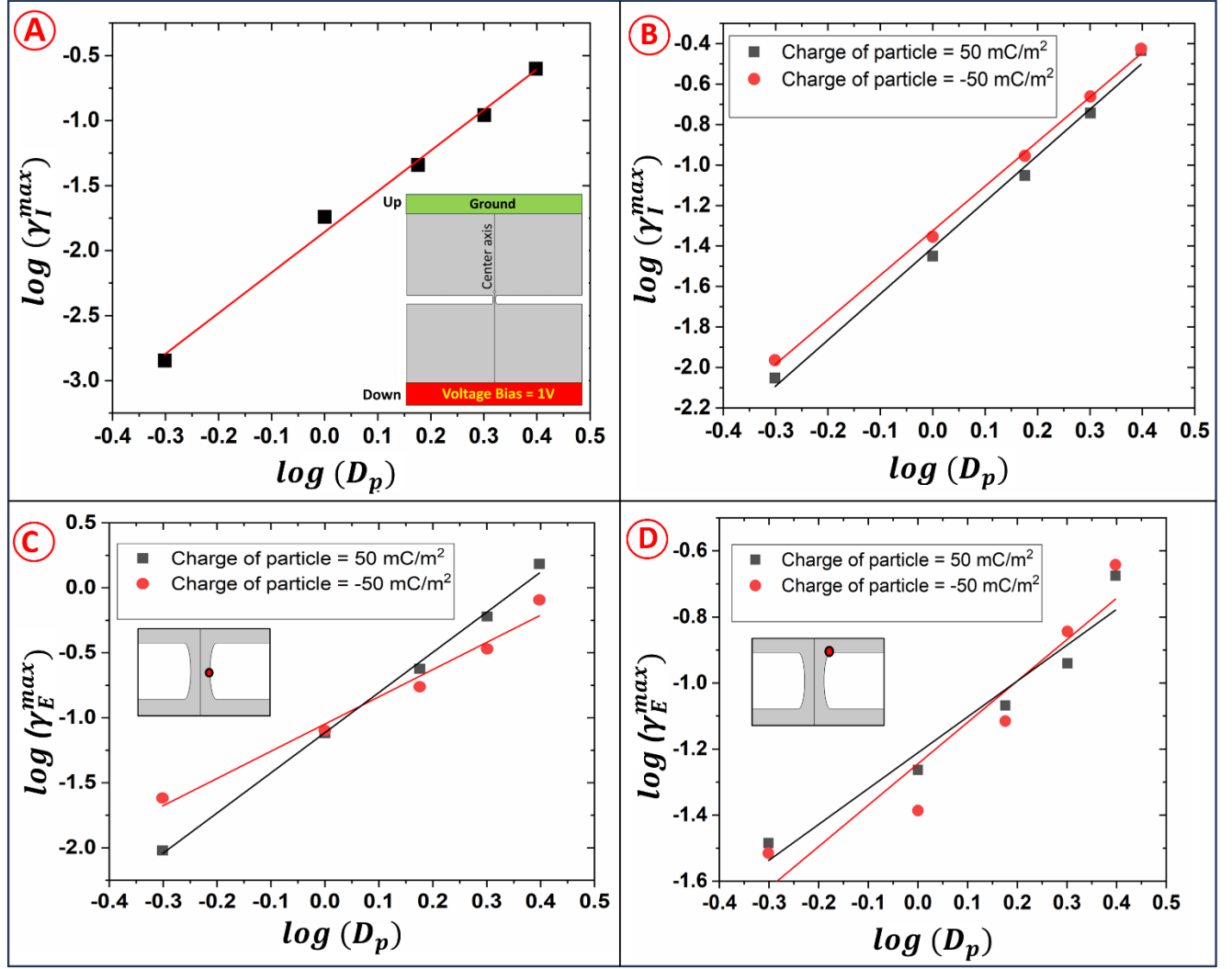


Figure 3. Size scaling for ionic current blockade and electric field sensing A) The linear fitted log-log plot of γ_I^{\max} as a function of particle diameter for uncharged particle and uncharged pore. The inset gives schematic illustration of the direction of voltage bias in the system B) comparative analysis of changes in γ_I^{\max} for particle of different size and charges polarities with linear fitting. pore charge of SiNx is -23mC/m² C) Scaling of γ_E^{\max} as a function of diameter of particle realized from center sensor (inset) D) Scaling of γ_E^{\max} as a function of diameter of particle realized from top edge sensor (inset). The case of γ_E^{\max} from bottom edge sensor is provided in SI Figure 6.

To study the effect of particle charge on the measured electric field, we conducted simulations of the translocation of a 2.5 nm diameter particle with charge density varying from -200 to 200 mC/m². This range was chosen based on the reported values of surface charge density of biomolecules, such as the surface charge of B-DNA: -163 mC/m² ²⁷, Albumin: -22 mC/m² ²⁸, dsDNA: -150mC/m², Streptavidin: -17.1mC/m² and DNA origami structures:-12.9mC/m² ²⁹. **Figure 4A** presents a comparison between the ionic current and electric-field based measurements. The depicted electric field is derived from the top edge electric field sensor, as sensing the edge electric field is more practical compared to the center sensor.

As seen in **Figure 4A**, the ionic current blockade is equally sensitive to both positive and negative charge densities, i.e., the sensitivity curve is symmetric about the origin. However, we find that the electric field is more sensitive to positive charge density than negative ones. In fact, the contrast for negative charge densities is almost independent of the magnitude of the negative charge making this measurement sensitive only to cationic particles. This asymmetric sensitivity is not due to the pore surface charge [**SI Figure 7**]. However, changing the location of the sensor [**SI Figure 14 B**] or changing the direction of the external bias [**Figure 4B**, **SI Figure 8**] reverses this asymmetry. In other words, we can tune the selectivity of detection for cations or anions depending on the direction of applied external field, which is not possible with current blockade based method.

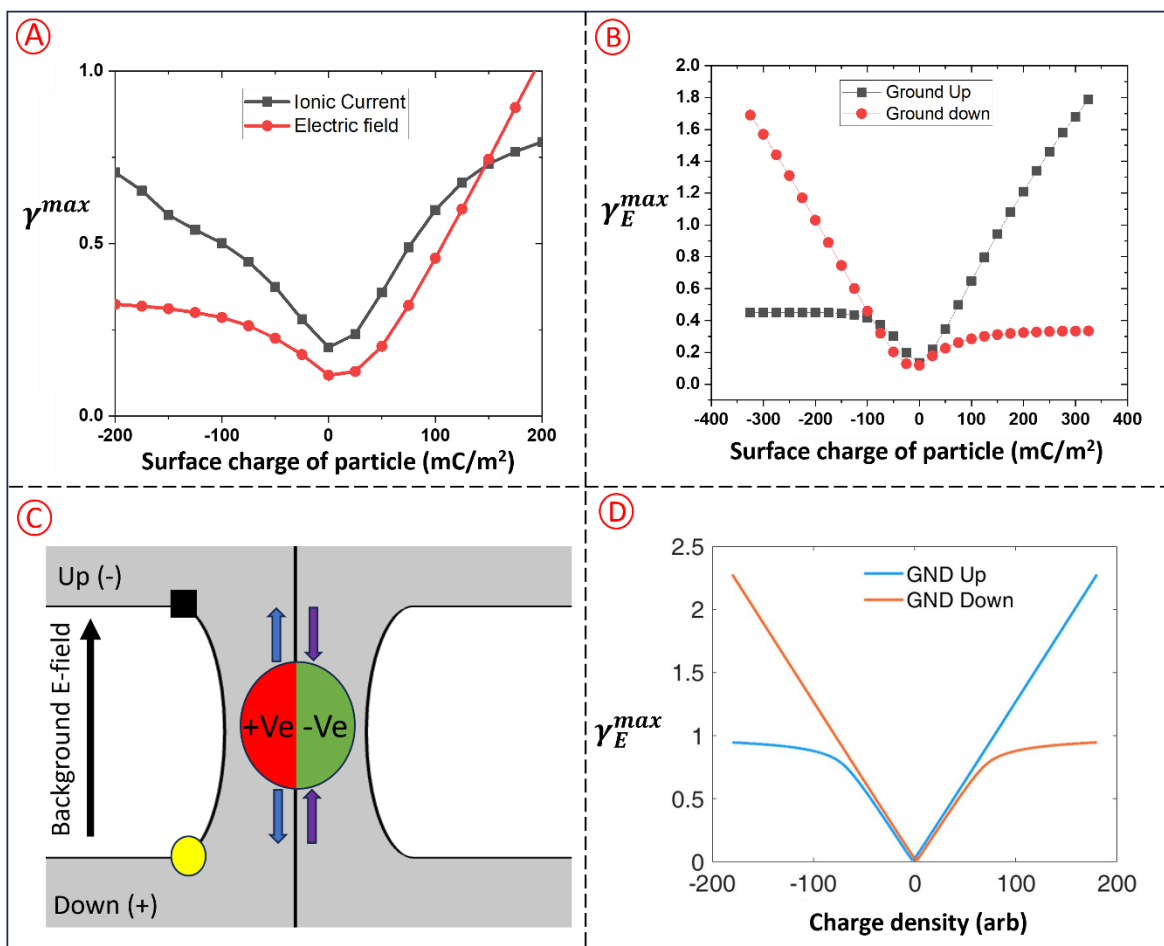


Figure 4. A) Comparative analysis of ionic current blockade and electric field modulations for Particles with different surface charges. The γ^{max} represents the general signal contrast. B) A schematic of directions of electric fields in the nanopore system. The black square and yellow circle represent the top and bottom edge E- field sensors. Arrows indicate the direction of electric field C) Reversal in electric field asymmetry upon altering the voltage bias direction; see Figure 3B for the schematic D) Model explaining the contrast reversal for varying particle charge.

The asymmetric charge sensitivity of nanopore electrometry originates from two factors. Firstly, there is a concentration of the electric field inside the nanopore due to spatial confinement [SI **Figure 9**]. Secondly, due to strong electrostatic screening, the field induced by the particle decays rapidly away from the it. These two factors combined with the fact that the direction of the electric field due to the particle flips its direction as it passes the electric field sensor [Figure 4C] leads to the asymmetry in the field sensitivity. Although the actual electric field distribution is quite complicated, one can capture the role of these factors in the observed asymmetry by using a simplified electrostatic model described in the section 4 in SI.

One of the major advantages of localized nanopore electrometry is to obtain translocation information simultaneously from multiple electric field sensors placed around the nanopore. For instance, one could have electric field sensors at both edges and as shown in **Figure 5**, due to the dependence of the total field on the sensor location [Section 4 in SI], these sensors provide different signal profiles for the same translocation event. The correlation of these two measurements can be used to reject spurious features that may occur in the data to reduce the error rate. Velocity fluctuations during translocation can limit the resolution in applications such as nanopore based sizing of DNA or proteins. The ability to do independent measurements as shown in **Figure 5** can enable self-referencing to compensate for these variations by explicitly measuring the start and end point of each event independently with two sensors. The ability to obtain self-referenced signals is a distinct feature of nanopore electrometry relative to current blockade based readout.

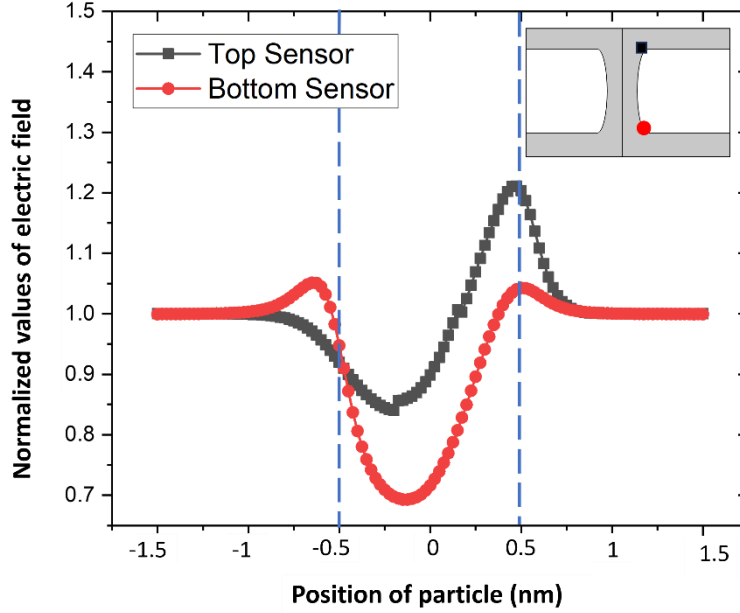


Figure 5: Electric field modulation during the translocation of particle with charge density of 50mC/m^2 , for sensors positioned near the pore (as shown in the inset). Sensors are color-matched with the respective curves in the plot. Dotted lines indicate the entry and exit of the nanopore reflected in the signal. Simultaneous measurements from multiple sensors at different locations exhibit different responses whose correlations can facilitate error correction.

Conclusion

In this study, we have presented an exploratory Multiphysics simulation study to understand the potential of using electric-field modulations (nanopore electrometry) instead of ionic current blockades to measure nanopore translocations. Our findings from simulations indicate that electric field sensing demonstrates comparable capabilities to the existing ionic current blockade-based techniques. Moreover, it allows for the differentiation of particles and selective sensing based on polarity of particles. By placing multiple electric field sensors around the nanopore, we can achieve simultaneous and correlated measurements of translocation event of particles through the pore.

This has the potential to reduce error rates and can be used for internal signal calibration. Nanopore electrometry can, in principle, operate without liquid electrolytes, and therefore, opens up opportunities for direct monitoring of air-borne particles and use in extreme environments such as outer space. The experimental realization of nanopore electrometry requires the availability of sensors that can respond to the local electric field. As we have mentioned, NV centers in nano-diamonds offers strong potential. Practical performance limits of nanopore electrometry will be set by the spatial and temporal resolution of electric-field measurements with these devices as well as potential cross-talk between multiple sensors in close proximity. However, being able to realize nanopore electrometry would enable the advantages described in this paper.

Impact of research in the advancement of knowledge or benefit to mankind

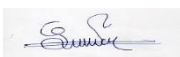
Nanopore sequencing has become a leading technique in next-generation DNA sequencing (NGS), significantly impacting various fields such as cancer research, COVID-19 detection, agri-genomics, microbiome studies, drug development, early disease detection, and practical biology education. While this technology has successfully scaled up DNA sequencing for commercial use, protein sequencing remains a distant goal due to its added complexity. Our work presents a novel approach by integrating electric field sensing with nanopore technology, enhancing its capabilities for multi-faceted detection and analysis. This advancement has wide-ranging applications, including the development of nanopore-assisted protein sequencing, early disease detection (e.g., neurodegenerative diseases), personalized medicine, and drug development. Hence, this work advances knowledge and also benefit mankind.

Author information

Corresponding Author

1. Muhammad Sajeer P - Center for Nanoscience and Engineering, Indian Institute of Science, Bangalore, India, 560012; <https://orcid.org/0000-0002-8093-713X> Email: muhammads@iisc.ac.in

Signature:



2. Manoj Varma- Center for Nanoscience and Engineering, Indian Institute of Science, Bangalore, India, 560012; <https://orcid.org/0000-0002-1218-1422> ; Email: mvarma@iisc.ac.in

Reference

1. Lee, K. *et al.* Recent Progress in Solid-State Nanopores. *Adv. Mater.* **30**, 1704680 (2018).
2. Taniguchi, M. Challenges of the practical applications of solid-state nanopore platforms for sensing biomolecules. *Appl. Phys. Express* **15**, 070101 (2022).
3. Karawdeniya, B. I., Bandara, Y. M. N. D. Y., Nichols, J. W., Chevalier, R. B. & Dwyer, J. R. Surveying silicon nitride nanopores for glycomics and heparin quality assurance. *Nat. Commun.* **9**, 3278 (2018).
4. He, L. *et al.* Digital immunoassay for biomarker concentration quantification using solid-state nanopores. *Nat. Commun.* **12**, 5348 (2021).
5. Zhang, K. *et al.* A nanopore interface for higher bandwidth DNA computing. *Nat. Commun.* **13**, 4904 (2022).
6. Dominic, A., Sajeer Parambath, M., Nasa, S. & Varma, M. Practical guide for in-house solid-state nanopore fabrication and characterization. *J. Vac. Sci. Technol. B* **41**, 043204 (2023).
7. Oxford Nanopore. <https://nanoporetech.com/>.

8. Wang, Y., Zhao, Y., Bollas, A., Wang, Y. & Au, K. F. Nanopore sequencing technology, bioinformatics and applications. *Nat. Biotechnol.* **39**, 1348–1365 (2021).
9. Li, M.-Y. *et al.* Revisiting the Origin of Nanopore Current Blockage for Volume Difference Sensing at the Atomic Level. *JACS Au* **1**, 967–976 (2021).
10. MacCoss, M. J. *et al.* Sampling the proteome by emerging single-molecule and mass spectrometry methods. *Nat. Methods* **20**, 339–346 (2023).
11. Arima, A., Tsutsui, M., Washio, T., Baba, Y. & Kawai, T. Solid-State Nanopore Platform Integrated with Machine Learning for Digital Diagnosis of Virus Infection. *Anal. Chem.* **93**, 215–227 (2021).
12. Yang, W. & Dekker, C. Single-Molecule Ionic and Optical Sensing with Nanoapertures. in *Single Molecule Sensing Beyond Fluorescence* (eds. Bowen, W., Vollmer, F. & Gordon, R.) 367–387 (Springer International Publishing, 2022). doi:10.1007/978-3-030-90339-8_12.
13. Chou, Y.-C., Masih Das, P., Monos, D. S. & Drndić, M. Lifetime and Stability of Silicon Nitride Nanopores and Nanopore Arrays for Ionic Measurements. *ACS Nano* **14**, 6715–6728 (2020).
14. Wilmsdorff, J. von, Kirchbuchner, F., Fu, B., Braun, A. & Kuijper, A. An experimental overview on electric field sensing. *J. Ambient Intell. Humaniz. Comput.* **10**, 813–824 (2019).
15. Bian, Sizhen. Human Activity Recognition with Field Sensing Technique. 37516 KB, VII, 202 pages (Technische Universität Kaiserslautern, 2022). doi:10.26204/KLUEDO/6922.
16. Noras, M. A. Activity Detection and Recognition With Passive Electric Field Sensors. *IEEE Trans. Ind. Appl.* **58**, 800–806 (2022).
17. Tang, X. & Mandal, S. Indoor Occupancy Awareness and Localization Using Passive Electric Field Sensing. *IEEE Trans. Instrum. Meas.* **68**, 4535–4549 (2019).

18. Rajasekar, R. & Robinson, S. Nano-electric field sensor based on Two Dimensional Photonic Crystal resonator. *Opt. Mater.* **85**, 474–482 (2018).
19. Han, Z., Xue, F., Hu, J. & He, J. Micro Electric Field Sensors: Principles and Applications. *IEEE Ind. Electron. Mag.* **15**, 35–42 (2021).
20. Bian, K. *et al.* Nanoscale electric-field imaging based on a quantum sensor and its charge-state control under ambient condition. *Nat. Commun.* **12**, 2457 (2021).
21. Dolde, F. *et al.* Electric-field sensing using single diamond spins. *Nat. Phys.* **7**, 459–463 (2011).
22. Hollendonner, M. *et al.* Quantum sensing of electric field distributions of liquid electrolytes with NV-centers in nanodiamonds. *New J. Phys.* **25**, 093008 (2023).
23. Ying, C., Houghtaling, J. & Mayer, M. Effects of off-axis translocation through nanopores on the determination of shape and volume estimates for individual particles. *Nanotechnology* **33**, 275501 (2022).
24. Van Oeffelen, L. *et al.* Ion Current Rectification, Limiting and Overlimiting Conductances in Nanopores. *PLOS ONE* **10**, e0124171 (2015).
25. Wang, C., Sensale, S., Pan, Z., Senapati, S. & Chang, H.-C. Slowing down DNA translocation through solid-state nanopores by edge-field leakage. *Nat. Commun.* **12**, 140 (2021).
26. Hu, R. *et al.* Solid-State Quad-Nanopore Array for High-Resolution Single-Molecule Analysis and Discrimination. *Adv. Mater.* **35**, 2211399 (2023).
27. Kominami, H., Kobayashi, K. & Yamada, H. Molecular-scale visualization and surface charge density measurement of Z-DNA in aqueous solution. *Sci. Rep.* **9**, 6851 (2019).

28. Öberg, C. M. & Rippe, B. Quantification of the electrostatic properties of the glomerular filtration barrier modeled as a charged fiber matrix separating anionic from neutral Ficoll. *Am. J. Physiol.-Ren. Physiol.* **304**, F781–F787 (2013).
29. Yamamoto, Y., Kominami, H., Kobayashi, K. & Yamada, H. Surface charge density measurement of a single protein molecule with a controlled orientation by AFM. *Biophys. J.* **120**, 2490–2497 (2021).